CROATICA CHEMICA ACTA
CCACAA, ISSN 0011-1643, e-ISSN 1334-417X
Croat. Chem. Acta **83** (1) (2010) 49–54.
CCA-3389

Original Scientific Paper

The Solidification Path of the Complex Metallic Al-Mn-Be Alloy*

Boštjan Markoli,[a,] Tonica Bončina,[b] and Franc Zupanič[b]**

[a]*Naravoslovnotehniška fakulteta, Univerza v Ljubljani, Aškerčeva 12, 1000 Ljubljana, Slovenija*
[b]*Fakulteta za strojništvo, Univerza v Mariboru, Smetanova 17, 2000 Maribor, Slovenija*

RECEIVED SEPTEMBER 19, 2008; REVISED MAY 19, 2009; ACCEPTED JULY 24, 2009

Abstract. The solidification paths of the $Al_{86.1}Mn_{2.5}Be_{11.4}$ and $Al_{84}Mn_{5.1}Be_{10.9}$ alloys, melt spun, cast into a copper mould and controlled cooled (during DSC) were investigated by means of light-optical microscopy (LOM), differential scanning calorimetry (DSC) combined with thermogravimetry (TG) or simultaneous thermal analysis (STA), scanning electron microscopy (SEM), transmission electron microscopy (TEM), Auger electron spectroscopy (AES) and the X-ray diffraction (XRD) line in Elletra Trieste, Italy. The constitutions of samples from both alloys were examined in all three states, *i.e.*, after melt spinning, after casting into a copper mould and after differential scanning calorimetry. It was established that in the cast and controlled-cooled specimens the alloys consisted of an aluminium-rich α_{Al}-matrix, and the Al_4Mn and Be_4AlMn phases. In the case of casting and DSC the primary crystallization began with the precipitation of the Be_4AlMn phase, followed by what can most likely be characterized as a uni-variant binary eutectic reaction $L \rightarrow (Be_4AlMn + Al_4Mn)$. The solidification process continued with an invariant ternary eutectic reaction, where the remaining melt (L) formed the heterogeneous structure ($\alpha_{Al} + Al_4Mn + Be_4AlMn$) or a ternary eutectic. When extremely high cooling rates were employed, as is the case with melt-spinning, the constituting phases of both alloys were precipitated in a very small form and the Be_4AlMn phase was completely absent in the form of primary polygonal particles and replaced by the icosahedral quasicrystalline phase or the *i*-phase. There was also no evidence of the Al_4Mn phase. The distribution, size and shape of all the constituents in the melt-spun alloys also varied from the contact surface towards the free surface of the ribbons. The smallest constituents were established at the contact surface, measuring less than 0.1 μm, to 0.5 μm at the free surface. The grains of the aluminium-rich matrix had mean diameters of less than 20 μm, close to the free surface, down to 1 μm at the contact surface.

Keywords: complex Al-Mn-Be alloys, metallography, solidification

INTRODUCTION

Investigations of aluminium-based alloys that contain quasicrystalline (QC) phases or have the ability to form them have become popular in recent years[1] due to the very special and promising properties of QC phases[2–7] *i.e.* the possibility to use them as particle reinforcement for alloys. Nevertheless, there is still a lot of fundamental research work to be done in order to fully understand the ability of aluminium-based alloys to form QC phases when different synthesis processes are employed. This calls for investigations in the area of solidification processes that are not fully explored due to the very complex nature of the binary (Al-Mn, Al-Be, Mn-Be)[8] and ternary Al-Mn-Be systems[9] and the fact that alloys from this ternary system are prone to form metastable crystalline phases as well as QC phases. A lot of effort has been put into research on the structure of QC phases[10–12] and attempts to predict which alloys will form such phases. Several research groups have also done a lot of work on the deformation of QC phases. Just recently, the possibility to employ QC phases in alloys for the automotive industry and studies of QC particles' interactions with an aluminium-based matrix have also been investigated. It is obvious that the formation of QC phases and their potential for applications are currently very interesting topics, which was the motivation for us to try to explain the solidification paths for the aluminium-based alloys containing manganese and beryllium.

EXPERIMENTAL

The alloys were synthesised from pure Al and Mn, and an $AlBe_5$ master alloy using vacuum induction melting and casting. The chemical compositions of the synthesised alloys were checked using ICP-AES (Inductively Coupled Plasma, Atomic Emission Spectroscopy) and

* Presented at the EU Workshop "Frontiers in Complex Metallic Alloys", Zagreb, October 2008. Dedicated to Professor Boran Leontić on the occasion of his 80th birthday.

** Author to whom correspondence should be addressed. (E-mail: bostjan.markoli@ntf.uni-lj.si)

the following compositions, expressed in mass fractions (w), were obtained: 90.6 % Al, 5.4 % Mn and 4.0 % Be for the $Al_{86.1}Mn_{2.5}Be_{11.4}$ alloy and 88.4 % Al, 10.88 % Mn and 0.71 % Be for the $Al_{84}Mn_{5.1}Be_{10.9}$ alloy.

Melts of both the synthesised alloys were then cast into a copper mould and melt spun on a melt spinner (30M, Marko Inc). The graphite crucibles were protected with BN on their inner surfaces to prevent any contamination of the melt. The crucible had a cover, with the space above the melt filled with pure Ar (flow rate approximately 4 l/min) to obtain an overpressure relative to the pressure of the chamber, where nitrogen was used as a protective gas (flow rate approximately 25 l/min). The wheel speed of the melt spinner was varied between 19.6 m/s and 25.2 m/s.

The preparation of samples for the LOM, SEM and AES followed standard mechanical metallographic procedures. Special attention was given to the deep-etching and particles-extraction techniques to reveal the morphology of the phases and to give clues about the course of the solidification process.

Simultaneous thermal analyses (STA), including DSC and thermogravimetry (TG), were performed in an STA 449 Jupiter between 500 °C and 1100 °C, with heating and cooling rates of 10 °C/min in nitrogen. However, only the DSC results will be presented in this paper.

The energy dispersive spectroscopy (EDS) was applied in both the SEM and TEM. However, here it should be noted that any determination of the amount of beryllium using EDS detectors is very difficult and unreliable since the fluorescence yield of beryllium is very low and the absorption of its radiation in the sample is very strong. Therefore, the chemical compositions of the phases containing beryllium were reliably determined by employing Auger electron spectroscopy (AES) in a Microlab 310-F.The energy of the primary electrons was 10 keV, the electron current was 10 nA and the electron-beam diameter was 10 nm. The specimens were etched with argon ions for approximately 1.5 h to remove the surface oxide layer prior to the analyses. The results of the AES analyses are not included in this paper.

The X-ray diffraction (XRD) was carried out on a Siemens D-5000, using Cu $K\alpha_1$ radiation, with a scan rate of 0.025°/s in the 2Θ range of 20° to 80° and at XRD1-beamline (Elettra, Sincrotrone Trieste, Italy) using X-rays with a wavelength of 0.1 nm in a transmission mode.

THEORETICAL BACKGROUND

To follow up the course of solidification for the Al-Mn-Be alloys it is necessary to critically evaluate the existing binary and ternary phase diagrams, *i.e.* Al-Mn, Al-Be, Mn-Be and Al-Mn-Be. The published data offer information on binary Al-Mn and Al-Be, and limited information on Mn-Be[8] whereas the ternary diagram, *i.e.*, the Al-rich corner of that diagram, is available in Ref. 9. The binary Al-Be (see figure in Ref. 8, p. 94) is actually a border version of the eutectic-type phase diagram with the eutectic point shifted to the extreme left-hand side into the Al-rich corner, resulting in the appearance of a so-called degenerated eutectic structure. There is a very limited solid solution of beryllium in aluminium (fraction of Be atoms 0.007 %), whereas the beryllium is dissolved in aluminium in excess of 0.3 % at 644 °C. Apart from these features this system turns out to be more or less the simplest one of the three.

On the other hand, the binary Al-Mn phase diagram shows a complex structure, caused primarily by the manganese allotropic modifications and thus changes in its crystal and electron structure with increasing or decreasing temperature. This results in the appearance of numerous intermetallic compounds and high- and low-temperature phases and also yields a large number of equilibria, which in turn results in a complex diagram structure (see figure in Ref. 8, p. 132). This is also the first indicator that the constitution of the Al-Mn-Be ternary system might also be complex. The published data do not provide us with the binary phase diagram for Mn-Be as such, but there is information on the appearance of at least three intermetallic compounds, *i.e.* $Be_{12}Mn$, Be_2Mn and δ-Be_8Mn.

As we move towards the ternary Al-Mn-Be system, we can see that only a small portion of this system is covered, *i.e.* the Al-rich corner (see figure in Ref 9). The projection of the Al-rich corner shows the liquidus surface containing four troughs, three of them meeting at a ternary eutectic point E. There are also four regions of primary crystallization for α_{Al}, Be, $Be_2Mn_3Al_{15}$ and Al_6Mn. This is where the ambiguity sets in as the $Be_2Mn_3Al_{15}$ phase still has an unclarified crystal structure and stoichiometry, although Raynor discovered it in 1953. The Al_6Mn phase is supposed to be a stable one, emerging from the binary Al-Mn system, but in reality it scarcely appears in the microstructure of alloys from this portion of the ternary Al-Mn-Be system. Furthermore, considering the lack of clarity regarding the crystal structure of the $Be_2Mn_3Al_{15}$ phase, the newest literature[13] claims that during the pouring process into the permanent mould, the structure of this phase is hexagonal with a stoichiometry of $Be_2Mn_3Al_{15}$, although no evidence is provided for this. If this phase is to be a stable one, as stated by Ref. 8, then it should not appear when higher cooling rates are employed, *e.g.*, casting in a permanent mould. This also contradicts our own results regarding the presence and stoichiometry of the $Be_2Mn_3Al_{15}$ after employing slower and faster cooling rates during the casting.[14,15] Therefore, we decided to

explore the solidification path, constitution and morphology of the phases of Al-Mn-Be alloys at different cooling rates.

RESULTS AND DISCUSSION

The solidification path of the Al-Mn-Be alloys (varying the mass fractions of Mn from 5.4 to 10.88 %) was studied at three different cooling rates, ranging from the slowest to the fastest, *i.e.*, controlled cooling at 10 K/min (DSC), casting into a copper mould, and rapid quenching with melt spinning. The cooling rates for the casting into the copper mould and the melt spinning were not estimated as it is widely accepted that melt spinning yields the highest cooling rates known, ranging from 10^4 to 10^6 K/s. The cooling rates present during the casting into a permanent mould are considered to be of a moderate class, which means that they are much faster than those in the case of the DSC, and much slower than those in the case of the melt spinning.

Solidification Path during Rapid Quenching (Melt Spinning)

In the case of the melt spinning of Al-Mn-Be alloys a strong directional solidification prevailed, with a transition from directional to equiaxed solidification where the ribbons were thicker (Figure 1).

The extensive EDS, AES and XRD analyses definitely showed the presence of the icosahedral phase, or *i*-phase, and grains of α_{Al}. The evaluation of the microstructure of the melt-spun ribbons of the Al-Mn-Be alloys indisputably proved that the *i*-phase formed as a primary phase, followed by the nucleation and growth of the aluminium-based crystal grains of α_{Al}. So, when extremely high cooling rates are imposed on the melt of the Al-Mn-Be alloy it obviously follows the solidification path of an ordinary binary alloy, since the formation of Be_4AlMn and Al_4Mn (hexagonal phase) is prevented and the *i*-phase forms as a primary phase, followed by the nucleation and directional growth of the α_{Al}. As mentioned above, the directional growth of the α_{Al} changes into multi-directional or equiaxed when the ribbons are thicker, and there is also the presence of the binary structure (α_{Al} + *i*-phase) in between the grains of the α_{Al}.

Solidification Path at Moderate Cooling Rates (Casting into a Permanent Copper Mould)

When moderate cooling rates are present during the solidification process of the Al-Mn-Be alloys the solidification path becomes much more complicated, as can be seen from the microstructure in Figure 2. The SEM micrograph shows the presence of four phases and a binary eutectic (α_{Al} + *i*-phase). Besides that, the EDS and AES analyses also showed that the *i*-phase appears in two different forms, as a dendritic phase, with a star-like shape, and as small, rounded particles, as denoted in Figure 2. There is also a strong presence of the Be_4AlMn phase, which can obviously serve as a nucleation site or substrate for the formation and growth of the *i*-phase, Al_4Mn (hexagonal phase) and the α_{Al} phase.

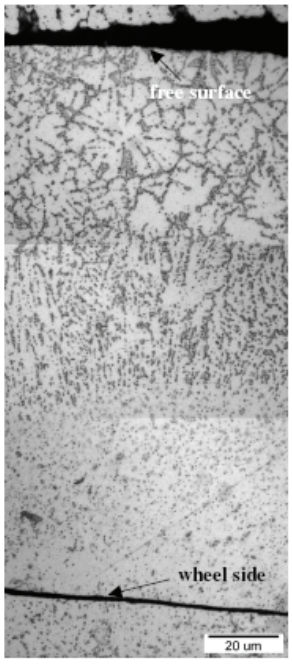

Figure 1. Composed LOM micrograph of the microstructure of the melt-spun Al-Mn-Be alloy (mass fractions: 5.4 % Mn and 4.0 % Be) ranging from the wheel-side to the upper free surface.

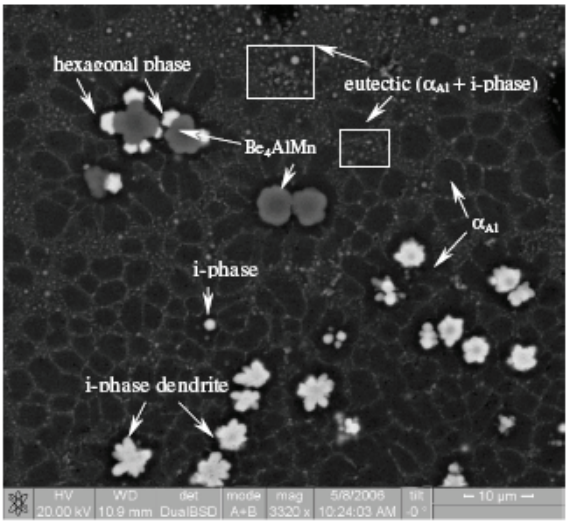

Figure 2. SEM micrograph of the microstructure for the Al-Mn-Be alloys containing 5.4 % Mn (mass fraction, *w*) after copper mould casting.

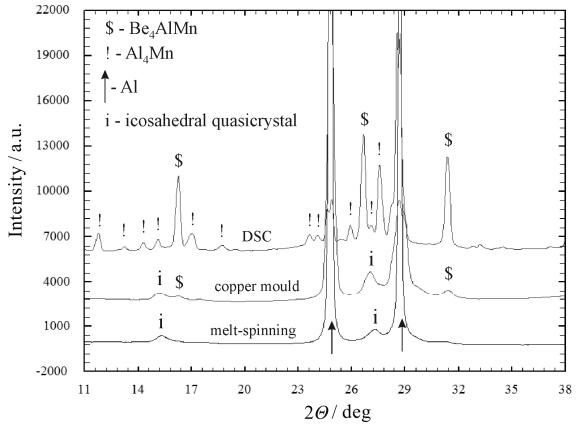

Figure 3. Comparison of the XRD patterns for all three cooling rates for the investigated Al-Mn-Be alloys.

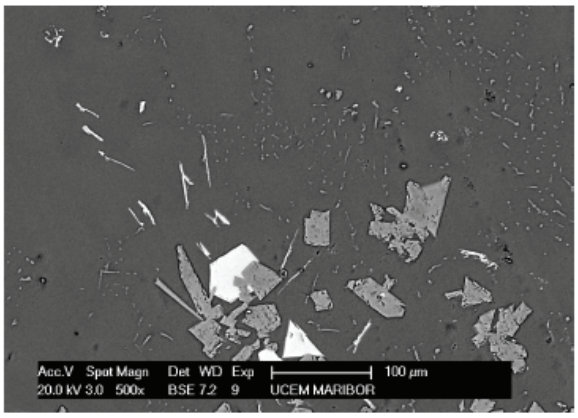

Figure 4. SEM micrograph of the microstructure for the Al-Mn-Be alloys containing 10.88 % Mn and 0.71 % Be (*w*) after DSC analysis.

Furthermore, Figure 2 offers evidence of the competition in the growth during the solidification process between the *i*-phase and Al_4Mn (hexagonal phase). This means that the conditions for the nucleation and growth of the phases and the solidification path itself are constantly shifting and changing as the solidification process goes forth, making it very difficult to accurately identify a realistic solidification path. Finally, there are large areas in Figure 2 that exhibit the fine structure of the binary eutectic (α_{Al} + *i*-phase), regardless of the fact that the Al-Mn-Be alloy is a ternary alloy where the solidification process usually ends with a ternary instead of a binary eutectic reaction.

The commented constitution of the Al-Mn-Be alloy was also checked with XRD, which verified the results of the other methods employed and confirmed the presence of the *i*-phase and the Be_4AlMn phase, as well as the hexagonal phase (Figure 3)

Based on the results presented for the copper mould casting we can conclude that the solidification begins with the formation of one of the phases, either the *i*-phase or the Be_4AlMn phase. This is immediately followed by the nucleation and growth of the other phase, and both then compete as they grow. During this the *i*-phase obviously creates the localized conditions for the nucleation and growth of the α_{Al} phase. This is because the growth of the *i*-phase depletes the surrounding melt with both the manganese and beryllium down to the maximum solubility in the molten aluminium, thus creating a perfect heterogeneous site for the nucleation and growth of the α_{Al} phase. The Be_4AlMn phase cannot only create the localized conditions for the α_{Al} phase nucleation and growth, but it also serves as a substrate for the nucleation and growth of the hexagonal phase. This is not surprising since the (111) planes for the Be_4AlMn phase and the (0001) planes for the Al_4Mn are reasonably close in the sense of interatomic distances.

From Figure 2 we can also see that the *i*-phase appears with two different morphologies, *i.e.*, dendritic and as rounded, small particles. These must form later in the solidification process when the crystallization itself is close to the end, which is when the formation and growth of the binary structure (α_{Al} + *i*-phase) sets in. Although the majority of the surrounding phase is the matrix of α_{Al}, apparently local differences in the temperature and the concentration of the elements appear, which are favourable sites for the nucleation and growth of small, rounded particles of the *i*-phase.

Solidification Path at Very Low Cooling Rates (DSC)

As we move towards the lowest cooling rate explored in this investigation (10 K/min, DSC) we can see that the microstructure is different once again from the previous two cases (permanent mould casting and melt spinning) for the 5.4 and 10.88 % Mn (*w*) in the alloy (Figure 4).

The microstructural constituents are much larger and well defined, regarding the surface morphology exhibiting facets. The hexagonal phase appears again with two different shapes as rectangular faceted particles as well as isolated lamella surrounded by the matrix of α_{Al}. Also, the faceted particles are much larger than in the previous cases, measuring well over 50 µm. The Be_4AlMn phase also has larger dimensions and comes in a very different shape compared to the permanent mould casting (Figure 2). This phase obviously forms a binary structure with the α_{Al}, which goes for the *i*-phase as well, only the amount of the binary structure (α_{Al} + hexagonal phase) is much lower in this case. The solidification path is again different compared to those with higher cooling rates, but it can be explained with more certainty.

From Figure 5 it is evident that in both alloys the primary crystallization begins with the nucleation and

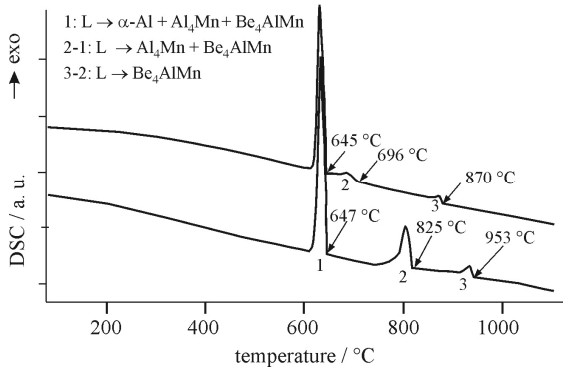

Figure 5. DSC analyses of the examined Al-Mn-Be alloys: cooling curve for the alloy with following mass fractions: 5.4 % Mn and 4.0 % Be (a) and alloy with 10.88 % Mn and 0.71 % Be (b).

growth of the Be_4AlMn phase (870 °C for 5.4 % Mn and 953 °C for 10.88 % Mn (*w*)), which also serves as a nucleation site for the hexagonal phase. The crystallization of the remaining melt then continues with the formation of a binary eutectic (Be_4AlMn + hexagonal phase) and a ternary eutectic (α_{Al} + Be_4AlMn + hexagonal phase) until all the melt is consumed. As expected, there is no evidence of the *i*-phase, since the cooling rates are obviously too low. The amount of hexagonal phase is the largest by far in the case of the DSC and decreases, as the cooling rates get higher because the formation of the *i*-phase sets in. The constitutions of the Al-Mn-Be alloys with three different cooling rates are assembled in Figure 3, where the XRD patterns for all three states are presented.

It is clear that the hexagonal phase, denoted as Al_4Mn, slowly disappears as the cooling rate increases, whilst the amount of *i*-phase grows with increasing cooling rate. The amount of Be_4AlMn is also reduced as the intensity of the peaks fades with the increasing cooling rate. The solidification path for the DSC case can thus be established, as presented in Figure 5 of the cooling diagram for the investigated Al-Mn-Be alloys.

All the reactions taking place are numbered from 1 to 3 and differ in terms of the temperature. These are higher when the manganese content in the alloy is higher. The solidification path is typical for the ternary alloys beginning with the primary crystallization of Be_4AlMn in this case. The solidification continues with a binary univariant reaction and ends with an invariant ternary eutectic reaction L→(α_{Al} + Be_4AlMn + hexagonal phase). There is no evidence of the formation of the *i*-phase, neither in the cooling curve (Figure 5) nor the associated microstructure (Figure 3).

CONCLUSION

From the results of the investigation of the solidification path for the Al-Mn-Be alloys at three different cooling rates the following can be concluded:

(i) The quasicrystalline icosahedral phase (*i*-phase) forms at cooling rates typical for permanent mould casting or higher. The *i*-phase does not appear at cooling rates usual for DSC analyses.

(ii) The amount of the hexagonal Al_4Mn phase decreases as the cooling rate increases, and it disappears completely at the highest cooling rates employed (melt spinning).

(iii) The amount of *i*-phase, on the other hand, grows and reaches a maximum during the melt spinning.

(iv) The solidification paths are different for all three cooling rates. The solidification path with the melt spinning is the simplest, where the primary nucleation and growth is associated with the formation of the *i*-phase and the solidification ends with a binary structure (αAl + *i*-phase). During the casting in the permanent mould the constitution is the most complex, containing four phases with different sizes and shapes, and a number of different structures. As the cooling rates decrease (DSC) the constitution of the Al-Mn-Be alloys changes and exhibits only three phases, but it is still not in compliance with the Al-rich corner of the "official" ternary system Al-Mn-Be.

Acknowledgements. The authors would like to thank Dr. Luisa Barba at Elettra Sinchrotrone Trieste, Italy for assistance with the XRD experiments.

REFERENCES

1. Hans-Rainer Trebin (Ed.), *Quasicrystals, Structure and Physical Properties*, Wiley-VCH GmbH&Co. KgaA, Weinheim, 2003.
2. J. Dolinšek, *Z. Kristallogr*. **224** (2009) 64–66.
3. V. Karpus, G. J. Babonas, A. Reza, S. Tumenas, H. Arwin, W. Assmus, and S. Brühne, *Z. Kristallogr*. **224** (2009) 39–41.
4. T. Takeuchi, *Z. Kristallogr*. **224** (2009) 35-37.
5. S. Bühler-Paschen, N. Lamquembe, V. Pacheco, F. Widder, E. Alleno, E. Bauer, U. Burkhardt, R. Cardoso Gil, O.Rouleau, W. Schnelle, B. Villeroy, Y. Grin, and C. Godard, 10th Int. Conf. on Quasicrystals, Zurich, 2008, *Program and Abstracts*, 2008, p. 36.
6. S. Ohhashi, A. Kato, and A. P. Tsai, 10th Int. Conf. on Quasicrystals, Zurich, 2008, *Program and Abstracts*, 2008, p. 125.
7. A. Singh, H. Somekawa, and T. Mukai, 10th Int. Conf. on Quasicrystals, Zurich, 2008, *Program and Abstracts*, 2008, p. 145.
8. *Binary Alloys Phase Diagrams*, 2nd ed., T. B. Massalski, H. Okamoto, P. R. Subramanian, L. Kasprzak (Eds.), ASM, Metals Park, Ohio 1990.
9. L. F. Mondolfo, *Aluminum Alloys: Structure and Properties*, London – Boston – Sydney – Wellington – Durban – Toronto Butterworths, London 1976.
10. C. Pay Gómez, 10th Int. Conf. on Quasicrystals, Zurich, 2008, *Program and Abstracts*, 2008, p. 130.
11. T. Weber and W. Steurer, *Z. Kristallogr*. **223** (2009) 835–838.
12. K. Saitoh, T. Yokosawa, and A. P. Tsai, 10th Int. Conf. on Quasicrystals, Zurich, 2008, *Program and Abstracts*, 2008, p. 136.
13. S. H. Kim, G. S. Song, E. Fleury, K. Chattopadhyay, W. T. Kim, and D. H. Kim, *Philos. Mag. A*, **82** (2002) 1495–1508.
14. F. Zupanič, T. Bončina, A. Križman, W. Grogger, C. Gspan, B. Markoli, and S. Spaić, *J. Alloys Compd.* **452** (2008) 343–347.
15. F. Zupanič, T. Bončina, B. Šuštaršič, I. Anžel, and B. Markoli, *Mater. Charact.* **59** (2008) 1245–1251.

SAŽETAK

Način skrućivanja kompleksne metalne Al-Mn-Be legure

Boštjan Markoli,[a] Tonica Bončina[b] i Franc Zupanič[b]

[a]*Naravoslovnotehniška fakulteta, Univerza v Ljubljani, Aškerčeva 12, 1000 Ljubljana, Slovenija*
[b]*Fakulteta za strojništvo, Univerza v Mariboru, Smetanova 17, 2000 Maribor, Slovenija*

Načini skrućivanja $Al_{86.1}B_{2.5}$ $Be_{11.4}$ i $Al_{84}Mn_{5.1}Be_{10.9}$ legura dobivenih lijevanjem pri velikim brzinama hlađenja ("melt-spinning" metoda), u bakrenu kokilu i uz kontrolirano hlađenje (za vrijeme DSC) istraživani su metodama optičke mikroskopije (LOM), diferencijalno pretražne kalorimetrije (DSC) u kombinaciji s termogravimetrijom (TG) ili simultanom toplinskom analizom (STA), pretražne elektronske mikroskopije (SEM), transmisijske elektronske mikroskopije (TEM), spektroskopije Augerovih elektrona (AES) i rendgenske difrakcije (XRD). Konstituenti uzoraka iz obje legure su ispitivani za tri različita stanja, tj. nakon izrazito brzog hlađenja, lijevanja u bakrenu kokilu i nakon diferencijalno pretražne kalorimetrije. Utvrđeno je da su se uzorci legura u lijevanom i kontrolirano hlađenom stanju sastojali od aluminijem bogate α_{Al}-osnove, te $Al_{10}Mn_3$ i Be_4AlMn faza. U slučaju lijevanja i diferencijalno pretražne kalorimetrije primarna je kristalizacija započela precipitacijom B_4AlMn faze što se može najvjerojatnije okarakterizirati kao univarijantna binarna eutektička reakcija $L \rightarrow (Be_4AlMn + Al_{10}Mn_3)$. Proces skrućivanja je nastavljen s invarijantnom ternarnom eutektičkom reakcijom, gdje preostala talina (L) stvara heterogenu strukturu ($\alpha_{Al} + Al_{10}Mn_3 + Be_4AlMn$) ili ternarni eutektik. Kada su korištene izrazito velike brzine hlađenja, kao u slučaju "melt-spinning" metode, konstitutivne faze obiju legura su precipitirale u veoma malom obliku, a Be_4AlMn faza bila je potpuno odsutna u obliku primarnih poligonalnih čestica i zamijenjena je "icosahedral" kristaliničnom fazom ili *i*-fazom. Također nema dokaza o prisutnosti $Al_{10}Mn_3$ faze. Raspodjela, veličina i oblik svih konstituenata u brzo-hladećim legurama su se promijenili od kontakne površine prema slobodnoj površini trakica, s manje od 0.1 μm pa do 0.5 μm kod slobodne površine. Zrna aluminijem bogate osnove imala su, blizu slobodne površine, srednji promjer manji od 20 μm, a kod kontakne površine srednji promjer zrna se smanjio na 1 μm.